# Amplitude Scaling of Wavepackets in Turbulent Jets

Luigi A Antonialli, André V G Cavalieri, Oliver T Schmidt, Tim Colonius, Peter Jordan, Aaron Towne, Guillaume A Brès

# Amplitude Scaling of Wavepackets in Turbulent Jets

Luigi A. Antonialli *, and André V. G. Cavalieri†
*Aeronautics Technological Institute, São José dos Campos, Brazil*

Oliver T. Schmidt‡
*University of California, San Diego, California, USA*

Tim Colonius§
*California Institute of Technology, Pasadena, California, USA*

Peter Jordan¶
*Pprime Institute, France*

Aaron Towne‖
*University of Michigan, Ann Arbor, Michigan, USA*

Guillaume A. Brès**
*Cascade Technologies, Palo Alto, California, USA*

**This paper studies the amplitude of large-scale coherent wavepacket structures in jets, modeled by the parabolized stability equations (PSE). Linear PSE can retrieve the shape of the wavepackets, but linearity leads to solutions with a free amplitude, which has traditionally been obtained in an *ad hoc* manner using limited data. We systematically determine the free amplitude as a function of frequency and azimuthal wavenumber by comparing the fluctuation fields retrieved from PSE with coherent structures educed from large-eddy simulation data using spectral proper orthogonal decomposition (SPOD). The wavepacket amplitude is shown to decay exponentially with Strouhal number for axisymmetric and helical modes at both Mach numbers considered in the study, 0.4 and 0.9. Analytical fit functions are proposed, and the scaled wavepackets provide reasonable reconstructions of pressure and velocity spectra on the jet centerline and lip-line over a range of streamwise positions.**††

*luigialbieri@gmail.com
†Assistant Professor, Aeronautic Engineering Division, andre@ita.br.
‡Assistant Professor, Department of Mechanical and Aerospace Engineering, oschmidt@ucsd.edu.
§Professor, Department of Mechanical and Civil Engineering, colonius@caltech.edu.
¶Professor, Thermal Fluids and Combustion Department, peter.jordan@univ-poitiers.fr.
‖Assistant Professor, Department of Mechanical Engineering, towne@umich.edu.
**Director of Operations, Aeroacoustics, gbres@cascadetechnologies.com.
††A conference paper of this work with homonymous title was presented at 2018 AIAA/CEAS Aeroacoustics Conference at Atlanta, Georgia in June 26, 2018. AIAA 2018-2978.

## Nomenclature

| | | |
|---|---|---|
| $A$ | = | scaling factor |
| $a_j$ | = | amplitude captured my mode $j$ |
| $a(\xi)$ | = | hydrodynamic wavenumber |
| $C_a, C_b$ | = | exponential function coefficient |
| $c_0$ | = | ambient sound speed |
| $D$ | = | jet diameter |
| $E$ | = | error |
| $f, g$ | = | generic functions |
| $M$ | = | Mach number |
| $m$ | = | azimuthal wavenumber |
| $P$ | = | pressure fluctuation |
| $\mathbf{q}$ | = | flow variables |
| $\mathbf{q}'$ | = | flow fluctuations in the time domain |
| $\bar{\mathbf{q}}$ | = | time-averaged component of $\mathbf{q}$ |
| $\tilde{\mathbf{q}}$ | = | shape function of the fluctuation amplitude |
| $\hat{\mathbf{q}}_{pse}$ | = | Parabolic Stability Equations calculated fluctuation flow field in the frequency domain |
| $\hat{\mathbf{q}}_{spod}$ | = | flow fluctuations for the leading SPOD in the frequency domain |
| $r$ | = | radial coordinate |
| $St$ | = | Strouhal number |
| $T$ | = | temperature |
| $t$ | = | time |
| $U_j$ | = | jet exit velocity |
| $u_r$ | = | radial velocity |
| $u_x$ | = | axial velocity |
| $u_\theta$ | = | azimuthal velocity |
| $W$ | = | Chebyshev quadrature weights |
| $W'$ | = | diagonal weight matrix |
| $x$ | = | axial coordinate |
| $\beta$ | = | normalised projection coefficient |
| $\gamma$ | = | heat capacity ratio |
| $\theta$ | = | azimuthal coordinate |

$\lambda$ = Spectral Proper Orthogonal Decomposition eigenvalue

$\rho$ = density

$\phi$ = polar coordinate

$\psi_j$ = basis functions of $\mathbf{q}'$

$\omega$ = angular frequency of the fluctuations

Subscripts

0 = nozzle exit

$f$ = end of analyzed domain

Superscripts

$H$ = Hermitian transpose

## I. Introduction

Jet noise remains a challenging problem in the aerospace community, due to increasingly stringent noise-emission regulations. Historically it was thought that the main source of sound in jet flows was related to small eddies (Laurence [1]) associated with turbulence, but more recently, large-scale structures have been shown to be a dominant source of sound. These structures initially grow exponentially through the Kelvin-Helmholtz mechanism, reach a peak, and then decay downstream, forming a wavepacket. Wavepackets have been observed and studied extensively; further information can be found in Jordan & Colonius [2] and Cavalieri *et al.* [3] and references therein.

Wavepacket models have been developed to predict the behaviour of large-scale turbulent structures in jets and their associated noise. The parabolized stability equations (PSE), described by Herbert [4] and Malik [5], were initially used to describe laminar-turbulent transition in slowly-diverging flows. But as shown in Gudmundsson & Colonius [6] and Sasaki *et al.* [7], PSE can be used to model coherent structures in turbulent jets, especially in the near-nozzle region characterised by amplitude growth. Central in such comparisons is spectral proper orthogonal decomposition (SPOD) of flow fluctuations, as described in Picard & Delville [8] and Lumley [9]. As recently shown by Towne *et al.* [10], the leading SPOD mode is expected to match the optimal flow response when white-noise forcing is considered, and this optimal response can be obtained using PSE for flows with strong convective amplification, as first pointed out by Jeun *et al.* [11]. This provides a basis to understand why PSE results compare favorably with the leading SPOD mode of jets.

Linear PSE has solutions with free amplitudes, which must be scaled with results from experiments or numerical simulations. This can be done in an *ad hoc* manner using a limited number of available measurements, or in a more theoretically-consistent manner by obtaining the amplitude of the Kelvin-Helmholtz mode near the nozzle exit by a projection using the adjoint mode (Rodríguez *et al.* [12]). Each combination of Strouhal number $St$ and azimuthal mode $m$ leads to a free amplitude. How such amplitudes scale with $St$ and $m$ remains an open question. If one wishes to

predict spectra of flow fluctuations using the aforementioned linear models, the frequency dependence of the amplitude is important. For lack of available information, Tam & Chen [13] assumed that wavepackets are excited by white noise in time and space. Similar hypotheses have been applied in linearised models used to model wall-bounded turbulence, but it is now known that the use of "coloured" excitation improves the agreement with reference data (Jovanovic & Bamieh [14], Chevalier *et al.* [15], Zare et al. [16]).

In the present study, we explore how initial wavepacket amplitudes change as a function of Strouhal number and azimuthal wavenumber. Empirical scaling laws of wavepacket amplitude are extracted from LES data, allowing us to infer how they may have been excited in the flow; possible candidates involve disturbances within the nozzle boundary layer (Kaplan *et al.* [17]) and/or non-linear interactions with other turbulent structures (Towne *et al.* [10]). The present analysis is intended to help to clarify the mechanisms underpinning the excitation of Kelvin-Helmholtz wavepackets.

To derive empirical scaling laws, we will use data from the large eddy simulations (LES) of Brès *et al.* [18, 19]. Because the LES provides full flow information, it is suitable for detailed comparisons with PSE results. Here, we identify the free amplitude of the PSE results by minimising the difference between the leading SPOD mode from the LES and the PSE solutions using a scalar amplitude variable. This allows us to explore how the free amplitude of the PSE wavepackets change with $St$, $m$, and Mach number, providing insight on the mechanisms by which wavepackets are excited.

This paper is organized as follows. In section II we present the LES results and the PSE model, and also describe how the free amplitude of PSE solutions can be found using the leading SPOD mode from LES data. In section III we show some validation results for PSE, then proceed with the determination of the wavepacket amplitudes as a function of $St$ and $m$, and we compare the spectrum using the identified amplitude function with LES and experimental results. The paper is completed with conclusions in section IV.

## II. Methods

### A. Large Eddy Simulation Database

This work relied on the numerical simulations described in Brès *et al.* [18, 20]. These are large eddy simulations (LES) of an isothermal subsonic jets, which exhaust from a converging-straight round nozzle, shown in figure 1. The boundary layer inside the nozzle is already turbulent; this was accomplished by synthetic turbulence injected at the position where a boundary layer trip was used in accompanying experiments. For the turbulent boundary layer, a wall model was used, as described in Brès *et al.* [21].

Simulations were performed for Mach numbers $M = \frac{U_j}{c_0} = 0.4$ and 0.9, based on jet exit velocity $U_j$ and ambient sound speed $c_0$. A range of Mach numbers 0.4, 0.7, 0.8 and 0.9 were simulated and validated against experimental measurements [18, 20]. Here, the focus is on the Mach 0.4 and 0.9 cases as representative of low and high-subsonic jets.

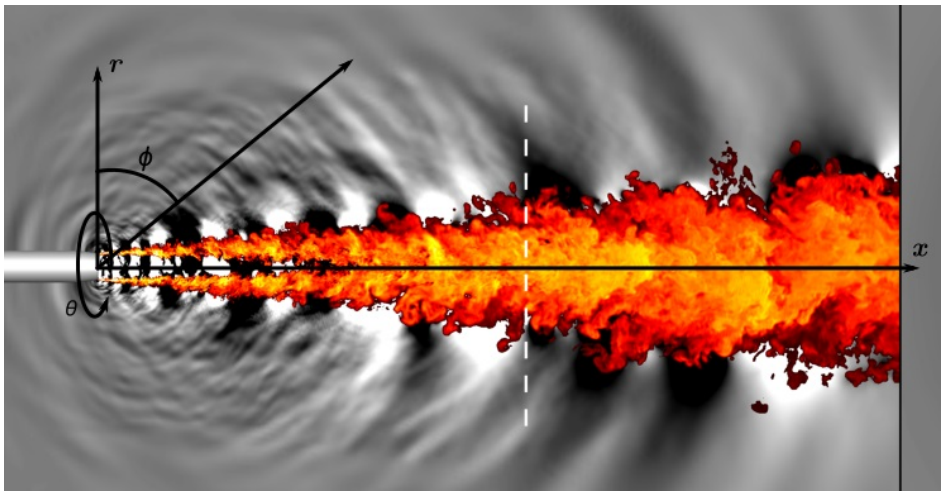


**Fig. 1 Jet LES simulation with coordinate system used throughout this work.**

The corresponding Reynolds numbers are $4 \cdot 10^5$ and $10^6$, respectively, using the jet diameter $D$ as the reference length; reference density and temperature are taken at the nozzle exit. The coordinate system used throughout this work is the same used in [18] and shown in figure 1, where $x$, $r$, $\theta$, and $\phi$ are the axial, radial, azimuthal, and polar coordinates, respectively, and the origin is at the center of the nozzle exit. All LES results are in close agreement with accompanying experiments, conducted at the Pprime Institute [18, 20, 22]. The measured turbulent flow spectra are broadbanded, and the LES results are in close agreement with experimental spectra up to a Strouhal number of 2.7.

### B. Spectral Proper Orthogonal Decomposition

To isolate the dominant wavepackets at each frequency and azimuthal wavenumber, spectral proper orthogonal decomposition (SPOD) was applied to the LES data. This procedure is explained in detail by Towne *et al.* [10]. For the round jets considered in this paper, SPOD decomposes the flow fluctuations into spatial modes that are function of $x$ and $r$ for each azimuthal wavenumber $m$, and Strouhal number $St$, i.e.,

$$\hat{\mathbf{q}}_{spod}(x, r, m, St) = \sum_{j=1}^{\infty} a_j(m, St)\psi_j(x, r, m, St). \tag{1}$$

The SPOD procedure expands the Fourier-transformed fluctuations $\hat{\mathbf{q}}_{spod}$ into orthogonal modes that optimally capture the flow energy. In eq. (1), $\psi_j$ are the basis functions of $\hat{\mathbf{q}}_{spod}$ and $a_j$ is the amplitude captured by the mode $j$. The total energy is recovered by the sum over $|a_j|^2$. For this work, only the first SPOD mode at each $St$, $m$ pair, is considered as it represents the leading wave-packet properties (Schmidt *et al.* [23]). The SPOD modes used here are those computed by Schmidt *et al.* [23].

### C. Parabolized Stability Equations

*1. Basic Equations*

The SPOD modes taken from the large-eddy simulation do not provide directly the amplitude of the Kelvin-Helmholtz wavepackets, as they also comprise other flow structures. For that matter, the Kelvin-Helmholtz component needs to be derived, and this is accomplished using the parabolized stability equations. The procedure is described in what follows.

The parabolized stability equations (PSE) are used to predict the fluctuation fields of the jet, using the mean turbulent field as a base flow. PSE was first developed by Bertolotti *et al.* [24] and unlike the traditional Orr-Sommerfeld equation, it can be used to study the linear stability of non-parallel flows with slow divergence in the streamwise direction, including jets. The PSE procedure was traditionally used for transitional flows, but as shown in various works (Gudmundsson & Colonius [6], Cavalieri *et al.* [25], Sasaki *et al.* [7]), it is also suitable for modeling large-scale structures in turbulent flows.

Considering flow variables written as $\mathbf{q}(x, r, \theta, t)$, it is possible to define a decomposition into an axisymmetric time-averaged component $\bar{\mathbf{q}}(x, r)$, which is used as base flow, and a temporal fluctuation component $\mathbf{q}'(x, r, \theta, t)$:

$$\mathbf{q}(x, r, \theta, t) = \bar{\mathbf{q}}(x, r) + \mathbf{q}'(x, r, \theta, t). \tag{2}$$

The vector $\mathbf{q}$ refers to the flow variables, $\mathbf{q} = (u_x, u_r, u_\theta, T, \rho)^T$, where $u_x$ is the axial velocity, $u_r$ radial velocity, $u_\theta$ azimuthal velocity, $T$ the temperature, and $\rho$ the density, all in cylindrical coordinates. The jet is non-swirling, so the mean azimuthal velocity component $\bar{u}_\theta$ is zero. The temporal fluctuation can be written as a Fourier decomposition in $\theta$ and $t$, show in equation (3).

$$\mathbf{q}'(x, r, \theta, t) = \sum_{\omega} \sum_{m} \hat{\mathbf{q}}_{pse}(x, r, m, St) e^{im\theta} e^{-i\omega t} \tag{3}$$

In Gaster [26] and Crighton & Gaster [27] an appropriate *Ansatz* for the fluctuations Fourier decomposition $\hat{\mathbf{q}}_{pse}$ is derived,

$$\hat{\mathbf{q}}_{pse}(x, r, m, St) = \tilde{\mathbf{q}}(x, r, m, St) e^{i \int_{x_0}^{x_f} \alpha(\xi) d\xi}. \tag{4}$$

In equation (4) the term $\alpha(\xi)$ is a complex-valued hydrodynamic wavenumber that varies with axial direction; its imaginary part is related to exponential growth or decay of fluctuations. $m$ is the azimuthal wavenumber, and $\omega$ is the angular frequency of the fluctuations. In this *Ansatz*, $\tilde{q}(x, r, m, St)$ is the shape function, which varies slowly in the streamwise direction, and the exponential term captures the fast variation related to exponential and oscillatory behaviour of the large-scale turbulent structures. The combination of these two parts generates fluctuations in the shape of a wavepacket.

To obtain the values of $\alpha(\xi)$ and $\tilde{\mathbf{q}}(x, r, m, St)$, the *Ansatz* from equation (4) is substituted into a matrix system with the linearized compressible equations of continuity, momentum, and energy, resulting in a system that can be cast in matrix form as

$$\left[A_M(\bar{\mathbf{q}}, \alpha, \omega, m) + B_M(\bar{\mathbf{q}})\right]\tilde{\mathbf{q}} + C_M(\bar{\mathbf{q}})\frac{\partial\tilde{\mathbf{q}}}{\partial x} + D_M(\bar{\mathbf{q}})\frac{\partial\tilde{\mathbf{q}}}{\partial r} = 0. \tag{5}$$

viscous terms were not considered due to the high Reynolds number of the jets considered. Details of the equation system can be found in Gudmundsson & Colonius [6] and Gudmundsson [28]. The PSE code used to generate the results is described in Sasaki *et al.* [7]. The initial fluctuation profile, in the nozzle exit plane, is given by linear stability theory, where the Kelvin-Helmholtz instability mode is found, and then marched downstream by the PSE. Note that other types of waves coexisting at the same frequency and azimuthal wavenumber, e.g., acoustic waves or disturbances growing through the Orr mechanism [29],[30], are not captured by PSE [31, 32], leading to a wavepacket dominated by the Kelvin-Helmholtz mode. For this case the base flow used is a time-averaged mean flow taken from the large eddy simulation, described in the previous section.

The domain was discretized numerically using 301 Chebyshev nodes in the $r$ direction, using the mapping function from Lesshafft & Huerre [33] to concentrate points in the jet region. The solution is advanced in the downstream $x$ direction using an implicit Euler method.

We are interested in determining the behavior of wavepacket amplitudes as a function of $St$ and $m$. To define these amplitudes in a consistent manner, the linear PSE solutions must be normalized in a definite way. We have adopted as normalization condition that flow fluctuations at the nozzle exit, $x = 0$, have unit norm. This is ensured by rescaling $\tilde{\mathbf{q}}_0 = \tilde{\mathbf{q}}(x = 0, r, m, St)$ such that

$$\tilde{\mathbf{q}}_0^H W' \tilde{\mathbf{q}}_0 = 1, \tag{6}$$

with $W'$ is diagonal weight matrix given by

$$W' = diag\left(W\bar{\rho}_0, W\bar{\rho}_0, W\bar{\rho}_0, W\frac{\bar{T}_0}{\gamma\bar{\rho}_0 M^2}, W\frac{\bar{\rho}_0}{\gamma(\gamma-1)\bar{T}_0 M^2}\right) \tag{7}$$

and where the superscript $H$ denotes the Hermitian transpose and the subscript 0 denotes properties at the nozzle exit. The matrix $W$ contains Chebyshev quadrature weights for integration over the radius. The inner product defined with $W'$ corresponds to the Chu norm used by Schmidt *et al.* [23]. The present definition thus normalises the PSE solution such that the initial Kelvin-Helmholtz mode, taken at $x = 0$, has unit norm.

### 2. *Study of Wavepacket Amplitudes Using PSE and SPOD Modes*

The normalization described in the previous section leads to an amplitude for the PSE solution that may not be representative of flow fluctuations for given $St$ and $m$, the PSE solutions require re-scaling using simulation data. The

values in the near-nozzle region of the jet were used to calculate a scaling factor between PSE results and the first SPOD mode educed from the LES data. This scaling factor $A$ is used to adjust the free amplitude of the linear PSE solutions, so as to minimise the difference $E$, given by

$$E = \|\sqrt{\lambda}\hat{\mathbf{q}}_{spod} - A\hat{\mathbf{q}}_{pse}\|, \tag{8}$$

where $\lambda$ is the SPOD eigenvalue, whose value is equal to the power spectral density (energy) of flow fluctuations for the corresponding SPOD eigenfunction. Rescaling the orthonormal SPOD modes by $\sqrt{\lambda}$ leads to amplitudes that are representative of the mode contribution to the full LES fields, as shown in Sinha *et al.* [34].

$A$ is a complex-valued scalar value, and its optimal value is obtained by minimising the error $E$ separately at each $m$ and $St$ combination. Setting the derivative of $E$ with respect to the amplitude $A$ to zero leads to

$$\langle\sqrt{\lambda}\hat{\mathbf{q}}_{spod}, \hat{\mathbf{q}}_{pse}\rangle - A\langle\hat{\mathbf{q}}_{pse}, \hat{\mathbf{q}}_{pse}\rangle = 0,$$

and thus the optimal amplitude is

$$A = \frac{\langle\sqrt{\lambda}\hat{\mathbf{q}}_{spod}, \hat{\mathbf{q}}_{pse}\rangle}{\langle\hat{\mathbf{q}}_{pse}, \hat{\mathbf{q}}_{pse}\rangle}. \tag{9}$$

The inner product in eq. (9) induces the norm in eq. (8), and thus defines the sense in which the error is minimized. Since $\hat{\mathbf{q}}_{spod}$ and $\hat{\mathbf{q}}_{pse}$ are functions of $x$ and $r$ and depend parametrically on $St$ and $m$, we define the inner product as

$$\langle f(r,x,St,m), g(r,x,St,m)\rangle = \int_{x_o}^{x_f}\int_0^{\infty}(f(x,r,St,m)g^*(x,r,St,m))r\,dr\,dx. \tag{10}$$

and consider only the pressure component in $\hat{\mathbf{q}}_{spod}$ and $\hat{\mathbf{q}}_{pse}$. This is due to a smoother behaviour of $A(St)$ observed when pressure is taken as the relevant flow quantity. However, considering velocity fluctuations or the full disturbance vector leads to similar results. Since azimuthal modes are orthogonal to each other, no azimuthal integration is required. This leads to an amplitude $A(St, m)$, depending on Strouhal number and azimuthal wavenumber. The argument of the complex-valued amplitude $A$ in eq. (9) also allows to set the phase of the PSE solution for a best match with the SPOD mode. It is possible to apply this method considering the whole domain, but, as illustrated in section III, the PSE has good agreement with the leading SPOD mode for a limited axial range for each Strouhal number $St$. Thus, limiting the domain will lead to more precise results. The trapezoid rule is used to calculate the integral in the inner product. PSE uses a different grid from the LES results, and therefore an interpolation was required to obtain values for the same $x$.

Unlike global stability modes, linear PSE does not provide a basis for flow fluctuations; PSE results are the solution of a boundary-value problem, with non-zero boundary conditions at the nozzle exit, and not eigenfunctions of a linear operator. Hence, strictly speaking, one cannot think of the procedure above as a projection as often done for stability

eigenfunctions (Rodríguez *et al.* [12, 35]). However, we are here interested in the determination of the amplitude of a single spatial function, and thus the approach can be used as a method to estimate wavepacket amplitudes considering a jet region between $x_o$ and $x_f$.

## III. Results

### A. Showing The PSE Results

The first step is to obtain PSE wavepackets and validate them by comparison with the first SPOD modes educed from the LES data. The PSE code was run for Mach numbers 0.4 and 0.9, for $St$ varying from 0.0488 to 1.6113 for the $M = 0.4$ case and from 0.0868 to 2.778 for the $M = 0.9$ case. These Strouhal number ranges were chosen due to the range of expected agreement between the PSE and the SPOD data ([6], [7]), so as to capture the exponential behaviour with less influence from fluctuations other than the Kelvin-Helmholtz wavepacket that show up in very low and high $St$. We thus focus on the parameter range with dominance of linear behaviour, justifying the neglect of non-linear terms in PSE.

The Strouhal numbers used are those of the SPOD results to facilitate comparison. The first three azimuthal modes are calculated ($m = 0, 1, 2$). A comparison of pressure fluctuations is shown for two representative $St$, and are restricted to the axisymmetric mode $m = 0$ for brevity. The Strouhal numbers are: $St = 0.44$ and 1.22 for $M = 0.4$, $St = 0.61$ and 1.39 for $M = 0.9$. The amplitude and phase of the PSE solution was adjusted using eq. (9). These results are shown in figure 2.

It is possible to see a close agreement between the PSE and the first SPOD modes for a good range of frequencies, especially in the upstream region, characterized by amplitude growth associated with the Kelvin-Helmholtz mechanism. For downstream points there is a growing mismatch, explored by Tissot *et al.* [30]. The present code was previously used by Sasaki *et al.* [36] and showed agreement for LES data Strouhal number as high as 4.

### B. Amplitude Scaling

Results from Sasaki *et al.* [36] are used to select appropriate integration limits in the definition of the inner product (10), which define the PSE solutions and SPOD modes are compared in determining the desired amplitudes. Sasaki *et al.* [36] showed a normalized projection coefficient $\beta$ between SPOD and PSE results at each $x$ station of the jet. The expression for $\beta$ is

$$\beta(x, St, m) = \frac{|\langle \mathbf{q}'_{spod}(x, r, St, m), \mathbf{q}'_{pse}(x, r, St, m)\rangle|}{||\mathbf{q}'_{spod}(x, r, St, m)||||\mathbf{q}'_{pse}(x, r, St, m)||} \tag{11}$$

where the inner product considers only radial integration in eq. (10) so as to indicate a local level of agreement at a station $x$. $\beta = 1$ is perfect agreement, and $\beta = 0$ is obtained when the PSE result at a given station, $x$ is orthogonal to the

corresponding SPOD result. Such agreement metric is shown in figure 3 for $M = 0.4$ and in figure 4 for $M = 0.9$.

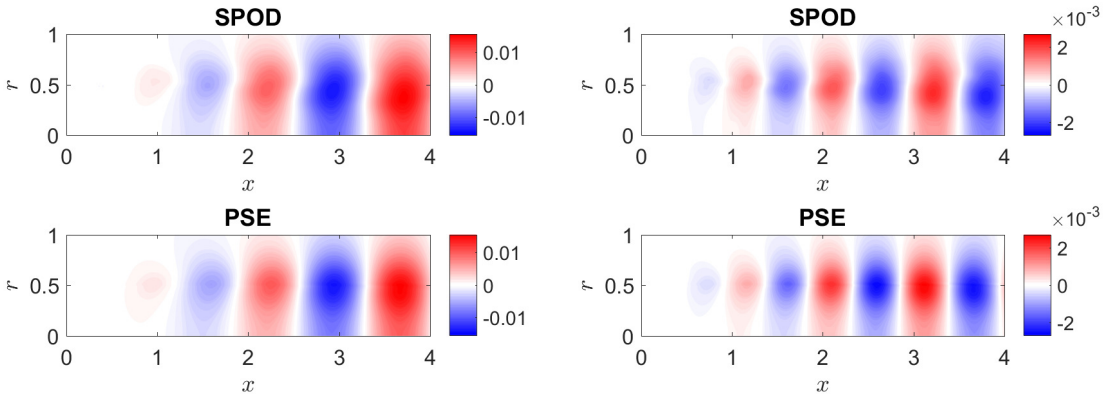


(a) $M = 0.4$, $St = 0.44$

(b) $M = 0.9$, $St = 0.61$

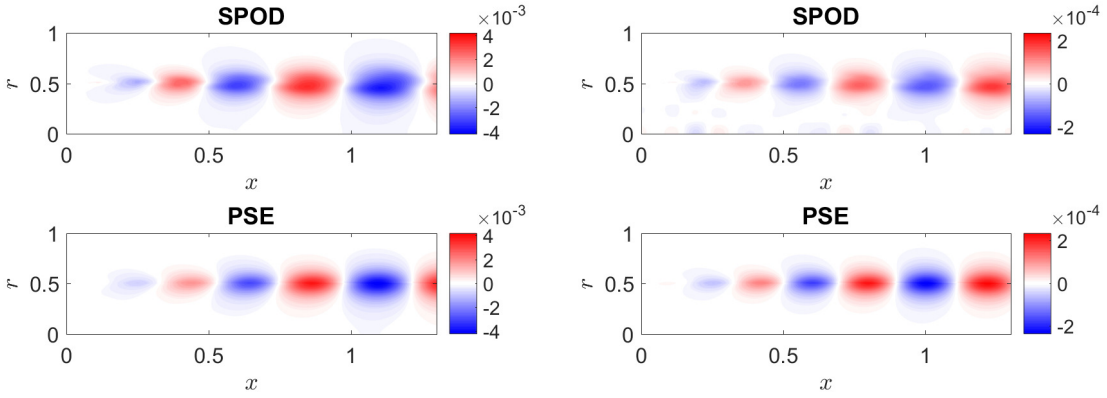


(c) $M = 0.4$, $St = 1.22$

(d) $M = 0.9$, $St = 1.39$

**Fig. 2 Pressure fluctuation contour for azimuthal mode $m = 0$ for Mach numbers $0.4$ and $0.9$, for two sample $St$ each.**

To ensure that the amplitude scaling is trustworthy, the region of the jet flow used is delimited by the yellow rectangle in figures 3 and 4; this upstream region corresponds to exponential growth of wavepackets associated with the Kelvin-Helmholtz mechanism [35], with good agreement between PSE and experimental or numerical results (Gudmundsson & Colonius [6], Cavalieri *et al.* [25], Tissot *et al.* [30], Sasaki et al. [36]). Therefore the range of the scaling will be $x/D \in [x_o = 0.5, x_f = 1.5]$, $St \in [0, 1.6]$ for $M = 0.4$ and $St \in [0, 2.5]$ for $M = 0.9$. The amplitude identification was performed for $M = 0.4$ and 0.9 and the first 3 azimuthal modes $m = 0, 1, 2$. These lower azimuthal wavenumbers are known to dominate the peak of far-field spectra [18, 37]. As commented earlier, the pressure fluctuations were used to obtain the amplitudes.

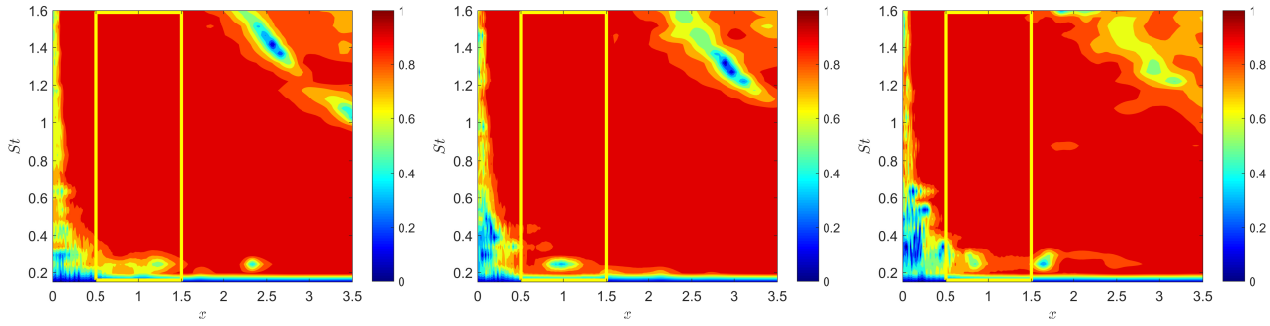


(a) $M = 0.4$, $m = 0$ (b) $M = 0.4$, $m = 1$ (c) $M = 0.4$, $m = 2$

**Fig. 3 Metric for agreement between SPOD mode and PSE for $m = 0, 1, 2$ for $M = 0.4$; Yellow rectangle indicates the region used for amplitude scaling in the present work.**

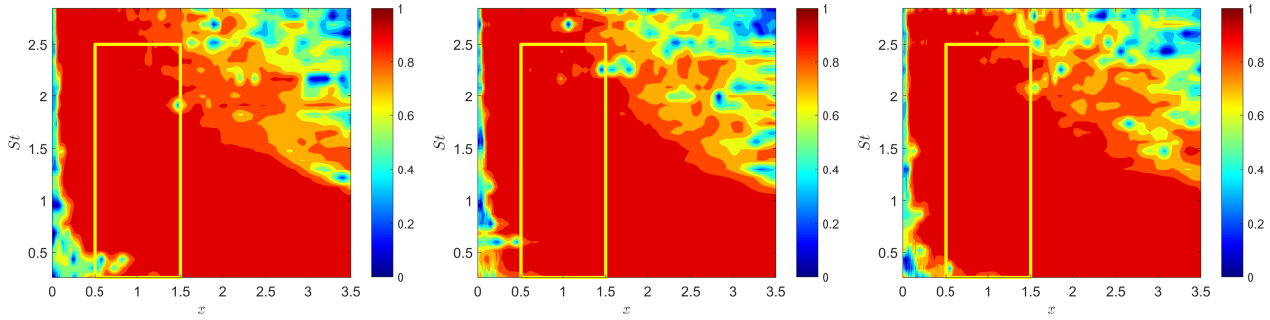


(a) $M = 0.9$, $m = 0$ (b) $M = 0.9$, $m = 1$ (c) $M = 0.9$, $m = 2$

**Fig. 4 Metric for agreement between SPOD mode and PSE for $m = 0, 1, 2$ for $M = 0.9$; Yellow rectangle indicates the region used for amplitude scaling in the present work.**

The absolute value of the amplitudes calculated using this choice of inner product are shown in figure 5 for $M = 0.4$ and $M = 0.9$. Even though observable oscillations are present in these plots, there is clearly an exponential decay of the absolute value of the amplitude with increasing of St. An exponential fit was applied to the data, yielding a function |A|(St) that may be used to scale the wavepacket models. The fitting function is given by

$$|A|(St) = Ce^{\kappa St} \tag{12}$$

with $C$ and $\kappa$ coefficients reported in table 1. The exponential fits are shown in figures 5 and 6, which refer to M=0.4 and 0.9, respectively. An accurate representation of the amplitude behaviour is obtained with the fitting functions. However, azimuthal mode $m = 2$ for the Mach 0.4 jet has more marked oscillations whose origin is unclear at this time. However, even in the latter case the general trend of amplitude decay with increasing $St$ is retrieved, with coefficients that are similar to the other cases.

**Table 1 Fit obtained from amplitude in function of $St$, where $C$ and $\kappa$ are the coefficients of the exponential equation $|A|(St) = Ce^{\kappa St}$.**

| $M$ | $m$ | $C$ | $\kappa$ |
|---|---|---|---|
| 0.4 | 0 | $1.85 \cdot 10^{-3}$ | $-2.02$ |
| 0.4 | 1 | $1.40 \cdot 10^{-3}$ | $-1.97$ |
| 0.4 | 2 | $8.42 \cdot 10^{-4}$ | $-1.60$ |
| 0.9 | 0 | $6.34 \cdot 10^{-4}$ | $-3.01$ |
| 0.9 | 1 | $5.10 \cdot 10^{-4}$ | $-3.05$ |
| 0.9 | 2 | $2.07 \cdot 10^{-4}$ | $-2.52$ |

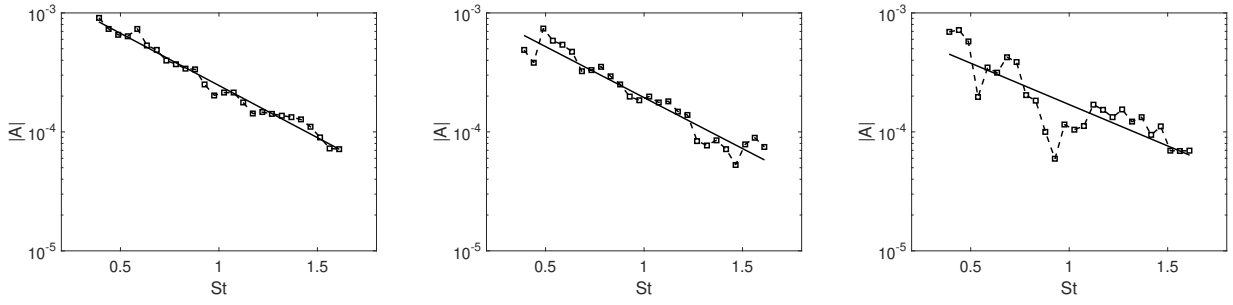


(a) $M = 0.4$, $m = 0$ (b) $M = 0.4$, $m = 1$ (c) $M = 0.4$, $m = 2$

**Fig. 5 Curve fit for scaling factor, in semilog scale, for $M = 0.4$. (−−) The original scaling factor obtained by eq. (9) with (□) the data points, and (−) the exponential fit of the black curve, with values shown in Table 1.**

Only the absolute value of $A$ is relevant, since the phase in a specific point is arbitrary due to the stochastic nature of the jet. The leading SPOD modes are eigenfunctions, and thus have arbitrary phase for each frequency; such phase is retrieved in the argument of $A$ and allows a visual comparison such as in fig. 2, but the precise value of phase is not of particular interest.

### C. Modeled Spectra

The Strouhal-number dependencies obtained in the previous section can be used to estimate power spectra at given positions of the flow; an accurate representation of spectra is a useful consistency check and shows whether the proposed exponential fits, once taken as initial PSE amplitudes, may describe accurately flow fluctuations for a range of St. Pressure spectra on the jet lipline and centerline were chosen to plot and compare the spectrum between the PSE model and the LES. These spectra are representative of near-field disturbances within the jet. Results are shown in figures 7-10. Figures 7 and 8 display centerline comparisons for M=0.4 and 0.9, respectively. Corresponding lipline spectra are shown in figures 9 and 10. Centerline comparisons are restricted to $m = 0$, as this is the sole azimuthal wavenumber with non-zero amplitude on the jet axis. Spectra on the lipline are shown for $m = 0$, 1 and 2.

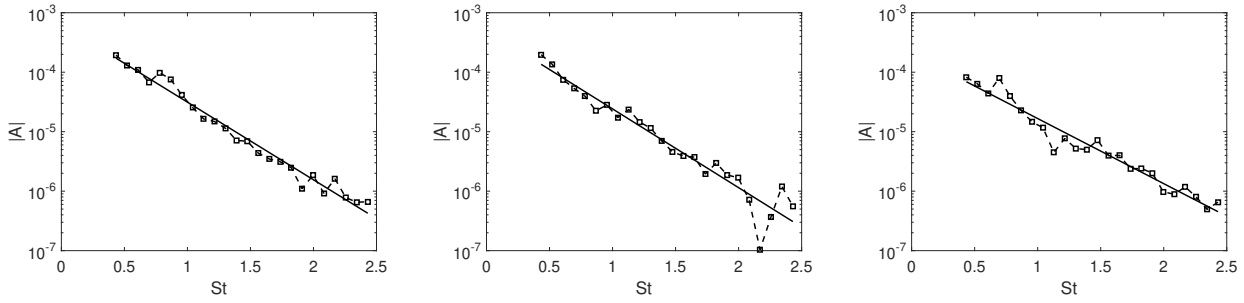


(a) $M = 0.9$, $m = 0$ (b) $M = 0.9$, $m = 1$ (c) $M = 0.9$, $m = 2$

**Fig. 6 Curve fit for scaling factor, in semilog scale, for $M = 0.9$. $(--)$ The original scaling factor obtained by eq. (9) with $(\square)$ the data points, and $(-)$ the exponential fit of the black curve, with values shown in Table 1.**

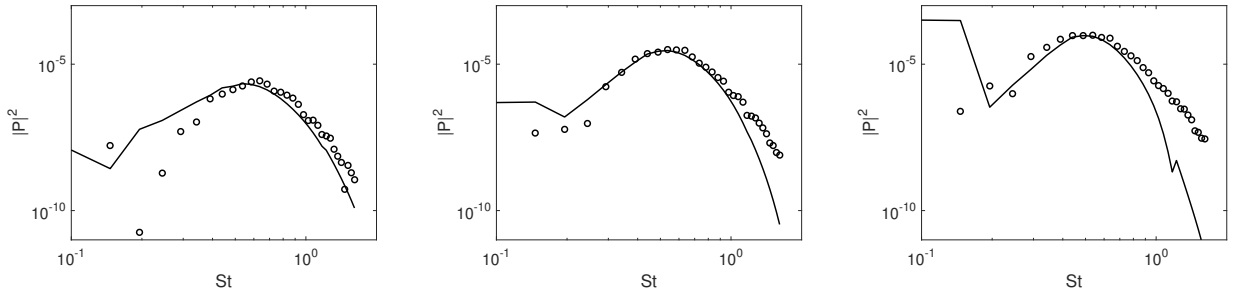


(a) $M = 0.4$ $m = 0$, $x/D = 1$ (b) $M = 0.4$ $m = 0$, $x/D = 2$ (c) $M = 0.4$ $m = 0$, $x/D = 3$

**Fig. 7 Centerline $(r/D = 0)$ spectrum using the scaling factor of pressure fluctuations, for the $M = 0.4$ case, for $m = 0$ and $x/D = 1, 2, 3$. $(-)$ PSE results, $(\circ)$ LES values.**

There is an overall good agreement between PSE results scaled with the amplitude fits in Table 1 and the pressure spectra, except for low Strouhal numbers, at which a mismatch between PSE and turbulent jet data can be associated with mechanisms other than Kelvin-Helmholtz (Schmidt *et al.* [23] & Lesshafft *et al.* [33]). For $St < 0.2$, some discontinuity appears, in view of the fact that the domain is not large enough.

For higher $St$ there is also a mismatch, possibly due to flow structures other than Kelvin-Helmholtz wavepackets with significant contributions at the considered positions. For the Mach 0.9 jet, oscillations in the spectra near the nozzle are observed; these are related to trapped acoustic waves (Towne *et al.* 2017 [38], Schmidt *et al.* [39]) which are not modelled in the PSE solution; however, the downstream spectra are dominated by the Kelvin-Helmholtz contribution and thus accurately represented by PSE with the amplitudes in Table 1.

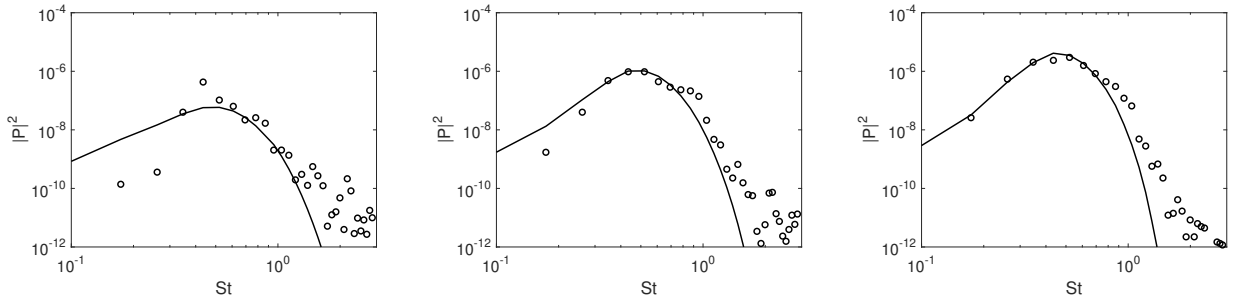


(a) $M = 0.9$ $m = 0$, $x/D = 1$ (b) $M = 0.9$ $m = 0$, $x/D = 2$ (c) $M = 0.9$ $m = 0$, $x/D = 3$

**Fig. 8 Centerline ($r/D = 0$) spectrum using the scaling factor of pressure fluctuations for the $M = 0.9$ case, for $m = 0$ and $x/D = 1, 2, 3$. (–) PSE results, (∘) LES values.**

Our results were obtained by considering solely pressure fluctuations in determination of the amplitude described in section II.C.2. The same approach was also applied considering the streamwise velocity $u_x$, and similar results were obtained;Similar trends can be seen in the comparison between the velocity spectrum of the scaled PSE and the experimental results by Cavalieri *et al.* [25], where good agreement is obtained again for the Mach 0.4 jet in figure 11.

The results show that the initial absolute value of the amplitude of turbulent jet wavepackets has an exponential dependence on $St$. Amplitudes change by about two orders of magnitude in the Strouhal range considered. It is thus clear that the excitation of wavepackets at the nozzle exit cannot be considered as white noise, with the same amplitude for all $St$. This can be further appreciated if a $St$-independent amplitude is considered for PSE; lipline $m = 0$ spectra generated with such an assumption are shown in figs. 12 and 13. Comparison of these figures to the amplitude-scaled results in figures 9 and 10 highlights that the exponential decay of amplitude with increasing St is an important dynamic feature, required to obtain spectral shapes accurately. Improvements on methods such as Tam & Chen [13] may be obtained if the observed exponential dependence in amplitude is included in models.

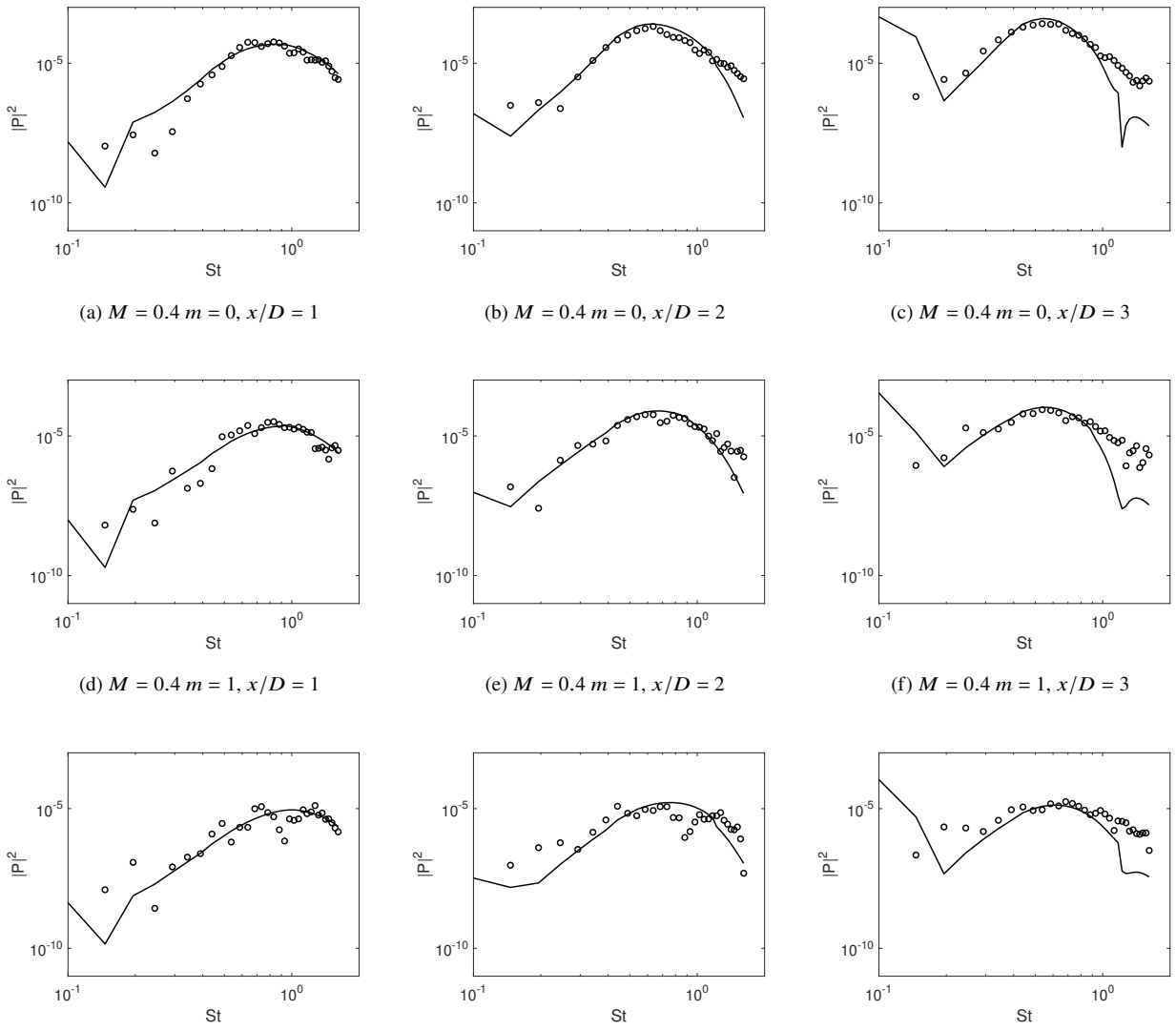


(a) $M = 0.4$ $m = 0$, $x/D = 1$ (b) $M = 0.4$ $m = 0$, $x/D = 2$ (c) $M = 0.4$ $m = 0$, $x/D = 3$

(d) $M = 0.4$ $m = 1$, $x/D = 1$ (e) $M = 0.4$ $m = 1$, $x/D = 2$ (f) $M = 0.4$ $m = 1$, $x/D = 3$

(g) $M = 0.4$ $m = 2$, $x/D = 1$ (h) $M = 0.4$ $m = 2$, $x/D = 2$ (i) $M = 0.4$ $m = 2$, $x/D = 3$

**Fig. 9 Lipline ($r/D = 0.5$) spectrum using the scaling factor of pressure fluctuations, for the $M = 0.4$ case, for $m = 0, 1, 2$ and $x/D = 1, 2, 3$. (−) PSE results, (∘) LES values.**

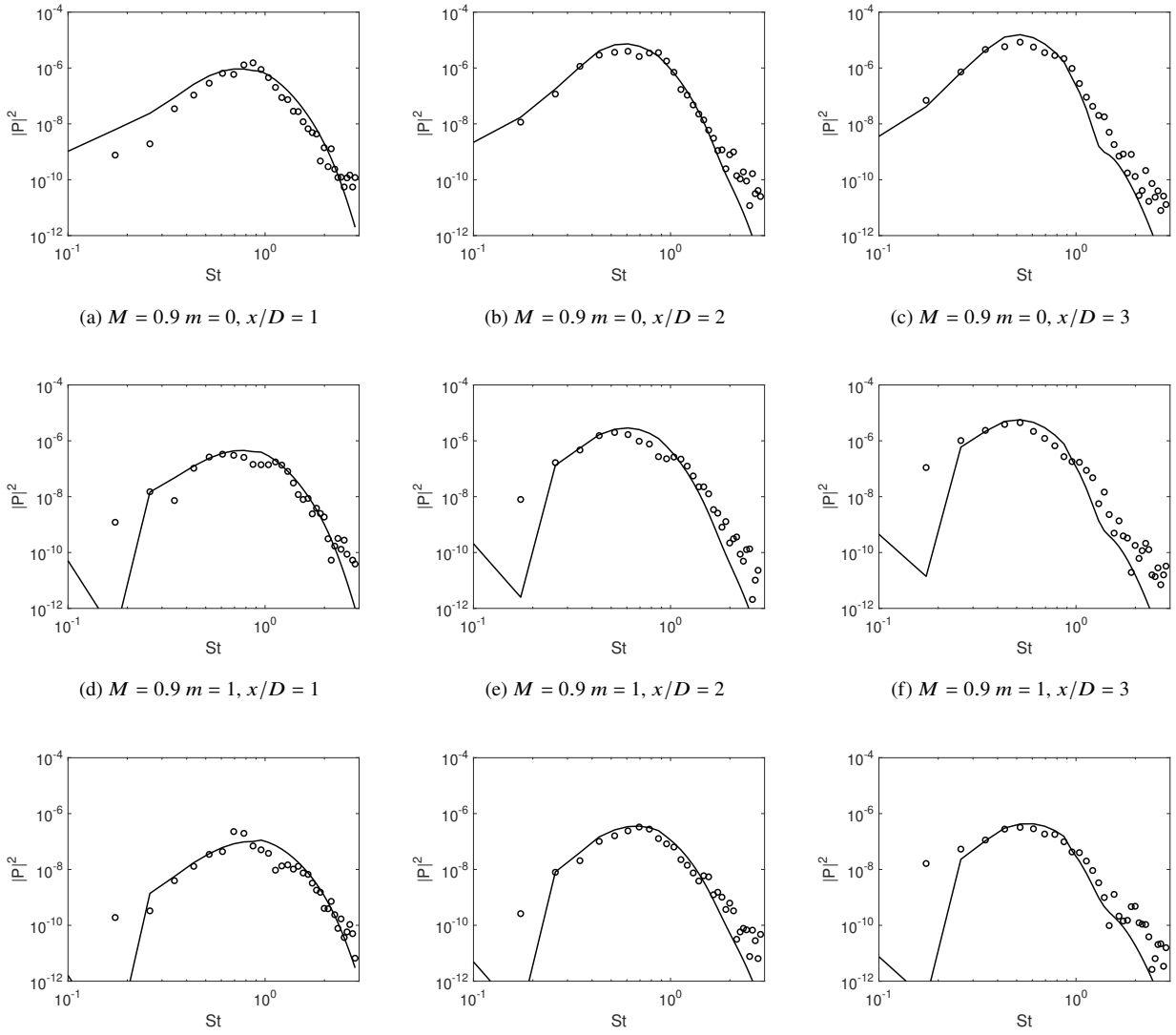


(a) $M = 0.9$ $m = 0$, $x/D = 1$ (b) $M = 0.9$ $m = 0$, $x/D = 2$ (c) $M = 0.9$ $m = 0$, $x/D = 3$

(d) $M = 0.9$ $m = 1$, $x/D = 1$ (e) $M = 0.9$ $m = 1$, $x/D = 2$ (f) $M = 0.9$ $m = 1$, $x/D = 3$

(g) $M = 0.9$ $m = 2$, $x/D = 1$ (h) $M = 0.9$ $m = 2$, $x/D = 2$ (i) $M = 0.9$ $m = 2$, $x/D = 3$

**Fig. 10 Lipline ($r/D = 0.5$) spectrum using the scaling factor of pressure fluctuations, for the $M = 0.9$ case, for $m = 0, 1, 2$ and $x/D = 1, 2, 3$. (−) PSE results, (∘) LES values.**

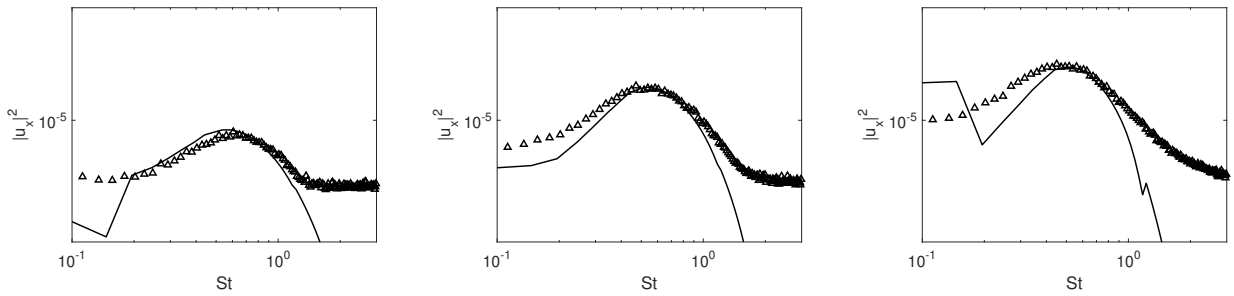


(a) $M = 0.4$ $m = 0$, $x/D = 1$ (b) $M = 0.4$ $m = 0$, $x/D = 2$ (c) $M = 0.4$ $m = 0$, $x/D = 3$

**Fig. 11 Centerline ($r/D = 0$) spectrum using the scaling factor of axial velocity fluctuations for the $M = 0.4$ case, for $m = 0$ and $x/D = 1, 2, 3$. (−) PSE results, (△) experimental data [25]).**

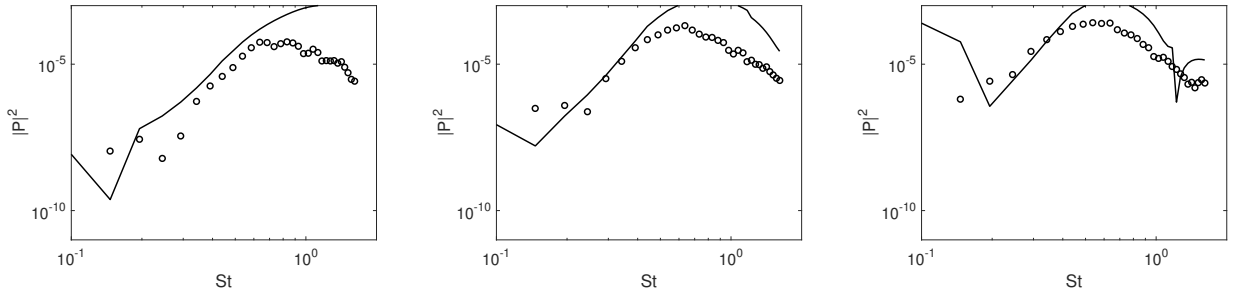


(a) $M = 0.4$ $m = 0$, $x/D = 1$ (b) $M = 0.4$ $m = 0$, $x/D = 2$ (c) $M = 0.4$ $m = 0$, $x/D = 3$

**Fig. 12 Lipline ($r/D = 0.5$) spectrum using a amplitude (white-noise forcing), taken for $St$=0.2 results for the $M = 0.4$ case, for $m = 0$ and $x/D = 1, 2, 3$. (−) PSE results, (○) LES values.**

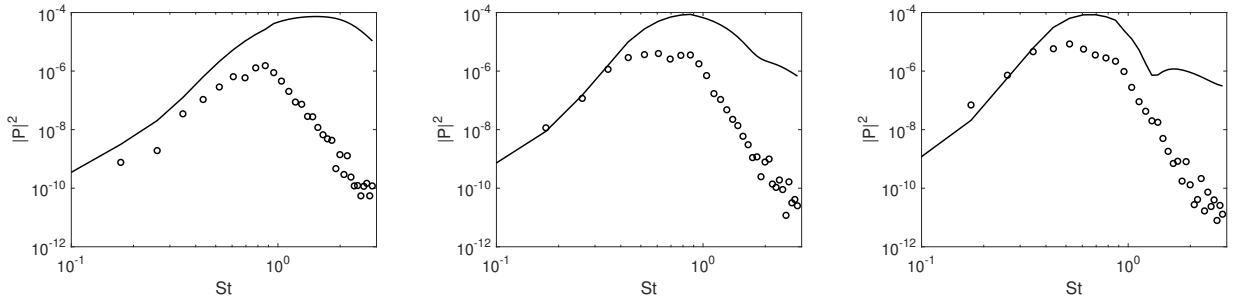


(a) $M = 0.9$ $m = 0$, $x/D = 1$ (b) $M = 0.9$ $m = 0$, $x/D = 2$ (c) $M = 0.9$ $m = 0$, $x/D = 3$

**Fig. 13 Lipline ($r/D = 0.5$) spectrum using a amplitude (white-noise forcing), taken for $St$=0.2 results for the $M = 0.9$ case, for $m = 0$ and $x/D = 1, 2, 3$. (−) PSE results, (○) LES values.**

## IV. Conclusion

The frequency dependence of turbulent jet wavepacket amplitudes is studied by an approach that consist in minimizing the difference in amplitude between linear PSE results and the leading SPOD mode educed from a well validated large-eddy simulation. This procedure, which is applied for a region of the flow where linear PSE has been shown to agree with numerical and experimental data, leads to wavepacket amplitudes with an exponential dependence on Strouhal number. Exponential fits are obtained for azimuthal wavenumbers $m = 0$, 1 and 2, for Mach numbers $M = 0.4$ and 0.9. These fits were shown to accurately predict in good agreement the power spectra of the flow, matching simulation and experimental data.

The amplitude scaling results may serve as a basis to study the receptivity mechanisms of Kelvin-Helmholtz wavepackets in turbulent jets. An open question regarding such wavepackets is related to their excitation; the exponential dependence seen here can serve as a test of proposed mechanisms and models, which should be able to reproduce the amplitude scaling observed in the present paper. The consistency of the same kind of fit for different Mach numbers is another indication of the clear exponential scaling of the wavepackets.

The next step is to understand how the wavepackets with this behavior are excited. In the current case, the turbulent boundary layer inside the nozzle is a clear candidate for an excitation mechanism; this has been explored by Kaplan *et al.* [17] but requires further study. The determination of the physical mechanism underpinning the observed exponential decay of amplitude with increasing $St$ is a future prospect of this work. The determination of amplitudes require use of LES data, and is thus an empirical determination of Kelvin-Helmholtz wavepacket amplitudes. Non-linear models (Wu & Huerre [40], Sandham & Salgado [41], Zhang & Wu [42]) may directly provide such amplitudes from first principles, especially if coupled to the nozzle boundary-layer dynamics.

The present results can be used to scale wavepacket models in jets if detailed data from experiment or simulation is not available; a recent example is the work of Wong et al. [43], where wavepacket source models with a proper amplitude scaling are used in an acoustic analogy to obtain broadband-shock-associated noise from supersonic jets. The present results may be used in acoustic predictions based on other kinematic source models jet wavepackets, such as in Papamoschou [44] or Maia *et al.* [45].

## Funding Sources

Luigi Antonialli had financial support from Capes by a Master´s degree scholarship. This project had funding from FINEP and Embraer through grant 137/18. The LES studies were supported by NAVAIR SBIR projects with computational resources provided by DoD HPCMP.

## Acknowledgments

The authors acknowledges Kenzo Sasaki for providing the data and code used in this paper, and ITA for supporting this project with the necessary resources.

## References

[1] Laurence, J. C., "Intensity, scale, and spectra of turbulence in mixing region of free subsonic jet," *NACA*, 1956.

[2] Jordan, P., and Colonius, T., "Wave packets and turbulent jet noise," *Annual review of fluid mechanics*, Vol. 45, 2013, pp. 173–195. doi:10.1146/annurev-fluid-011212-140756.

[3] Cavalieri, A., Jordan, P., and Lesshafft, L., "Wave-packet models for jet dynamics and sound radiation," *Applied Mechanics Reviews*, 2019. doi:/10.1115/1.4042736.

[4] Herbert, T., "Parabolized stability equations," *Annual Review of Fluid Mechanics*, Vol. 29, No. 1, 1997, pp. 245–283. doi:10.1146/annurev.fluid.29.1.245.

[5] Malik, M., Chuang, S., and Hussaini, M., "Accurate numerical solution of compressible, linear stability equations," *Zeitschrift für angewandte Mathematik und Physik ZAMP*, Vol. 33, No. 2, 1982, pp. 189–201. doi:10.1007/BF00944970.

[6] Gudmundsson, K., and Colonius, T., "Instability wave models for the near-field fluctuations of turbulent jets," *Journal of Fluid Mechanics*, Vol. 689, 2011, pp. 97–128. doi:10.1017/jfm.2011.401.

[7] Sasaki, K., Piantanida, S., Cavalieri, A. V., and Jordan, P., "Real-time modelling of wavepackets in turbulent jets," *Journal of Fluid Mechanics*, Vol. 821, 2017, pp. 458–481. doi:10.2514/6.2015-2214.

[8] Picard, C., and Delville, J., "Pressure velocity coupling in a subsonic round jet," *International Journal of Heat and Fluid Flow*, Vol. 21, No. 3, 2000, pp. 359–364. doi:10.1016/S0142-727X(00)00021-7.

[9] Lumley, J. L., *Stochastic tools in turbulence*, Courier Corporation, 2007.

[10] Towne, A., Schmidt, O. T., and Colonius, T., "Spectral proper orthogonal decomposition and its relationship to dynamic mode decomposition and resolvent analysis," *Journal of Fluid Mechanics*, Vol. 847, 2018, pp. 821–867.

[11] Jeun, J., Nichols, J. W., and Jovanović, M. R., "Input-output analysis of high-speed axisymmetric isothermal jet noise," *Physics of Fluids*, Vol. 28, No. 4, 2016, p. 047101. doi:10.1063/1.4946886.

[12] Rodríguez, D., Sinha, A., Brès, G. A., and Colonius, T., "Inlet conditions for wave packet models in turbulent jets based on eigenmode decomposition of large eddy simulation data," *Physics of Fluids*, Vol. 25, No. 10, 2013, p. 105107. doi:10.1063/1.4824479.

[13] Tam, C. K., and Chen, P., "Turbulent mixing noise from supersonic jets," *AIAA journal*, Vol. 32, No. 9, 1994, pp. 1774–1780. doi:10.2514/3.12173.

[14] Jovanovic, M., and Bamieh, B., "The spatio-temporal impulse response of the linearized Navier-Stokes equations," *Proceedings of the 2001 American Control Conference.(Cat. No. 01CH37148)*, Vol. 3, IEEE, 2001, pp. 1948–1953. doi:10.1109/ACC.2001.946026.

[15] Chevalier, M., Hœpffner, J., Bewley, T. R., and Henningson, D. S., "State estimation in wall-bounded flow systems. Part 2. Turbulent flows," *Journal of Fluid Mechanics*, Vol. 552, 2006, pp. 167–187. doi:10.1017/S0022112005008578.

[16] Zare, A., Jovanović, M. R., and Georgiou, T. T., "Colour of turbulence," *Journal of Fluid Mechanics*, Vol. 812, 2017, pp. 636–680. doi:10.1017/jfm.2016.682.

[17] Kaplan, O., Jordan, P., and Cavalieri, A. V., "Exploring the link between nozzle dynamics and wavepackets in a Mach 0.9 turbulent jet," *23rd AIAA/CEAS Aeroacoustics Conference*, 2017, p. 3708. doi:10.2514/6.2017-3708.

[18] Brès, G. A., Jordan, P., Jaunet, V., Le Rallic, M., Cavalieri, A. V., Towne, A., Lele, S. K., Colonius, T., and Schmidt, O. T., "Importance of the nozzle-exit boundary-layer state in subsonic turbulent jets," *Journal of Fluid Mechanics*, Vol. 851, 2018, pp. 83–124. doi:10.1017/jfm.2018.476.

[19] Brès, G. A., Ham, F. E., Nichols, J. W., and Lele, S. K., "Unstructured large-eddy simulations of supersonic jets," *AIAA Journal*, 2017. doi:10.2514/1.J055084.

[20] Brès, G. A., and Lele, S. K., "Modelling of jet noise: a perspective from large-eddy simulations," *Philosophical Transactions of the Royal Society A*, Vol. 377, No. 2159, 2019, p. 20190081. doi:10.1098/rsta.2019.0081.

[21] Brès, G. A., Ham, F. E., Nichols, J. W., and Lele, S. K., "Nozzle wall modeling in unstructured large eddy simulations for hot supersonic jet predictions," *AIAA paper*, Vol. 2142, 2013, p. 2013. doi:10.2514/6.2013-2142.

[22] Brès, G. A., Jaunet, V., Le Rallic, M., Jordan, P., Towne, A., Schmidt, O., Colonius, T., Cavalieri, A. V., and Lele, S. K., "Large eddy simulation for jet noise: azimuthal decomposition and intermittency of the radiated sound," *AIAA Paper*, Vol. 3050, 2016, p. 2016. doi:10.2514/6.2016-3050.

[23] Schmidt, O. T., Towne, A., Rigas, G., Colonius, T., and Brès, G. A., "Spectral analysis of jet turbulence," *Journal of Fluid Mechanics*, Vol. 855, 2018, pp. 953–982. doi:10.1017/jfm.2018.675.

[24] Bertolotti, F., Herbert, T., and Spalart, P., "Linear and nonlinear stability of the Blasius boundary layer," *Journal of Fluid Mechanics*, Vol. 242, 1992, pp. 441–474. doi:10.1017/S0022112092002453.

[25] Cavalieri, A. V., Rodríguez, D., Jordan, P., Colonius, T., and Gervais, Y., "Wavepackets in the velocity field of turbulent jets," *Journal of Fluid Mechanics*, Vol. 730, 2013, pp. 559–592. doi:10.1017/jfm.2013.346.

[26] Gaster, M., "On the effects of boundary-layer growth on flow stability," *Journal of Fluid Mechanics*, Vol. 66, No. 03, 1974, pp. 465–480. doi:10.1017/S0022112074000310.

[27] Crighton, D., and Gaster, M., "Stability of slowly diverging jet flow," *Journal of Fluid Mechanics*, Vol. 77, No. 02, 1976, pp. 397–413. doi:10.1017/S0022112076002176.

[28] Gudmundsson, K., "Instability wave models of turbulent jets from round and serrated nozzles," Ph.D. thesis, California Institute of Technology, 2010. doi:10.7907/BQH9-G487.

[29] Jiménez, J., "How linear is wall-bounded turbulence?" *Physics of Fluids*, Vol. 25, No. 11, 2013, p. 110814. doi:10.1063/1.4819081.

[30] Tissot, G., Zhang, M., Lajús, F. C., Cavalieri, A. V., and Jordan, P., "Sensitivity of wavepackets in jets to nonlinear effects: the role of the critical layer," *Journal of Fluid Mechanics*, Vol. 811, 2017, pp. 95–137. doi:10.2514/6.2015-2218.

[31] Towne, A., and Colonius, T., "One-way spatial integration of hyperbolic equations," *Journal of Computational Physics*, Vol. 300, 2015, pp. 844–861. doi:10.1016/j.jcp.2015.08.015.

[32] Towne, A., Rigas, G., and Colonius, T., "A critical assessment of the parabolized stability equations," *Theoretical and Computational Fluid Dynamics*, Vol. 33, No. 3-4, 2019, pp. 359–382. doi:10.1007/s00162-019-00498-8.

[33] Lesshafft, L., and Huerre, P., "Linear impulse response in hot round jets," *Physics of Fluids*, Vol. 19, No. 2, 2007, p. 024102. doi:10.1063/1.2437238.

[34] Sinha, A., Rodríguez, D., Brès, G. A., and Colonius, T., "Wavepacket models for supersonic jet noise," *Journal of Fluid Mechanics*, Vol. 742, 2014, pp. 71–95. doi:10.1017/jfm.2013.660.

[35] Rodríguez, D., Cavalieri, A. V., Colonius, T., and Jordan, P., "A study of linear wavepacket models for subsonic turbulent jets using local eigenmode decomposition of PIV data," *European Journal of Mechanics-B/Fluids*, Vol. 49, 2015, pp. 308–321. doi:10.1016/j.euromechflu.2014.03.004.

[36] Sasaki, K., Cavalieri, A. V., Jordan, P., Schmidt, O. T., Colonius, T., and Brès, G. A., "High-frequency wavepackets in turbulent jets," *Journal of Fluid Mechanics*, Vol. 830, 2017b. doi:10.1017/jfm.2017.659.

[37] Cavalieri, A. V., Jordan, P., Colonius, T., and Gervais, Y., "Axisymmetric superdirectivity in subsonic jets," *Journal of fluid Mechanics*, Vol. 704, 2012, pp. 388–420.

[38] Towne, A., Cavalieri, A. V., Jordan, P., Colonius, T., Schmidt, O., Jaunet, V., and Brès, G. A., "Acoustic resonance in the potential core of subsonic jets," *Journal of Fluid Mechanics*, Vol. 825, 2017, pp. 1113–1152. doi:10.1017/jfm.2017.346.

[39] Schmidt, O., Towne, A., Colonius, T., Cavalieri, A., Jordan, P., and Brès, G., "Wavepackets and trapped acoustic modes in a turbulent jet: coherent structure eduction and global stability," *Journal of Fluid Mechanics*, Vol. 825, No. 1, 2017, pp. 1153–1181. doi:10.1017/jfm.2017.407.

[40] Wu, X., and Huerre, P., "Low-frequency sound radiated by a nonlinearly modulated wavepacket of helical modes on a subsonic circular jet," *Journal of Fluid Mechanics*, 2009. doi:10.1017/s0022112009990577.

[41] Sandham, N. D., and Salgado, A. M., "Nonlinear interaction model of subsonic jet noise," *Philosophical Transactions of the Royal Society A: Mathematical, Physical and Engineering Sciences*, Vol. 366, No. 1876, 2008, pp. 2745–2760. doi:10.1098/rsta.2008.0049.

[42] Zhang, Z., and Wu, X., "Nonlinear evolution and acoustic radiation of coherent structures in subsonic turbulent free shear layers," *Journal of Fluid Mechanics*, Vol. 884, 2020. doi:10.1017/jfm.2019.909.

[43] Wong, M. H., Jordan, P., Honnery, D. R., and Edgington-Mitchell, D., "Impact of coherence decay on wavepacket models for broadband shock-associated noise in supersonic jets," *Journal of Fluid Mechanics*, Vol. 863, 2019, pp. 969–993. doi: 10.1017/jfm.2018.984.

[44] Papamoschou, D., "Wavepacket modeling of the jet noise source," *International Journal of Aeroacoustics*, Vol. 17, No. 1-2, 2018, pp. 52–69. doi:10.1177/1475472X17743653.

[45] Maia, I. A., Jordan, P., Cavalieri, A., and Jaunet, V., "Two-point wavepacket modelling of jet noise," *Proceedings of the Royal Society A*, Vol. 475, No. 2227, 2019, p. 20190199. doi:10.1098/rspa.2019.0199.